Aalborg Universitet

AALBORG UNIVERSITY
DENMARK

Controller Stability and Low-frequency Interaction Analysis of Railway Train-Network Systems

Kong, Rui; Sahoo, Subham; Blaabjerg, Frede; Lyu, Xiaoqin; Wang, Xiaoru

Published in:
2023 25rd European Conference on Power Electronics and Applications, EPE 2023 ECCE Europe

Publication date:
2023

Document Version
Accepted author manuscript, peer reviewed version

Link to publication from Aalborg University

Citation for published version (APA):
Kong, R., Sahoo, S., Blaabjerg, F., Lyu, X., & Wang, X. (2023). Controller Stability and Low-frequency Interaction Analysis of Railway Train-Network Systems. *2023 25rd European Conference on Power Electronics and Applications, EPE 2023 ECCE Europe*.

General rights
Copyright and moral rights for the publications made accessible in the public portal are retained by the authors and/or other copyright owners and it is a condition of accessing publications that users recognise and abide by the legal requirements associated with these rights.

- Users may download and print one copy of any publication from the public portal for the purpose of private study or research.
- You may not further distribute the material or use it for any profit-making activity or commercial gain
- You may freely distribute the URL identifying the publication in the public portal -

Take down policy
If you believe that this document breaches copyright please contact us at vbn@aub.aau.dk providing details, and we will remove access to the work immediately and investigate your claim.

Controller Stability and Low-frequency Interaction Analysis of Railway Train-Network Systems

Rui Kong[1], Subham Sahoo[1], Frede Blaabjerg[1], Xiaoqin Lyu[2], Xiaoru Wang[2]
[1]AAU Energy, Aalborg University
9220 Aalborg East, Denmark
Tel.: +45 / (0) – 5278 0150.
E-Mail: Ruko@energy.aau.dk
[2] School of Electrical Engineering, Southwest Jiaotong University
610031 Chengdu, China
Tel.: +86 / (0) – 028 6636 7992.
E-Mail: xrwang@home.swjtu.edu.cn

Keywords

«Railway vehicles», «AC-DC converter», «Small-signal stability», «Stability analysis», «Impedance analysis».

Abstract

In electrified railways, low-frequency oscillations (LFO) are commonly observed as a result of the widespread implementation of electric trains incorporating power electronic converters. While the impedance method has been employed in current stability studies for train-network systems, there is a requirement to extend stability modeling and analysis studies for the train-network system considering multiple trains having different control strategies. Hence, this paper establishes a unified impedance model in the dq-frame for the aforementioned system. Subsequently, an improved stability criterion, namly the dominant eigenvalue frequency response criterion (DEFRC), is proposed to assess system stability and unveil the mechanism of LFO. Furthermore, the interaction between different trains is clarified by analysis and case studies. Finally, the theoretical analysis is verified for accuracy based on time domain simulations.

Introduction

In recent years, due to the rapid development of electrified railways, the extensive utilization of single-phase power electronic converters has become prevalent in electric trains. The interaction between the train converters and the traction network may give rise to LFO [1], which can lead to severe accidents, such as traction blockades [2].

In accordance with the frequency-domain impedance modeling method [3], the train-network system is constructed by incorporating the input impedance of the trains and the output impedance of the traction network, thereby enabling the calculation of the impedance ratio for stability analysis [4]. The utilization of Park transform and small-signal linearization in the dq impedance modeling method has found extensive application in establishing the linear time-invariant (LTI) model for single-phase converters employing dq decoupling control (DQDC) [5], [6]. However, the transient direct current control (TDCC) of train converters is typically executed in single phase, with the corresponding linear time-invariant (LTI) impedance model commonly derived in the single-phase stationary frame [7], [8]. An impedance model is put forward for TDCC train converters in the dq frame [9], thereby achieving a unified approach with the existing impedance model of DQDC converters. To this end, the system stability with different trains was assessed by the generalized Nyquist criterion (GNC). Nevertheless, the GNC lacks of a well-defined indicator for the system stability margin and the ability to explain the mechanism driving LFO. Additionally, it cannot encompass the frequency response characteristics of the eigenvalues, which affects the intuitive identification of the oscillation frequency.

Furthermore, when considering mixed conditions that involve trains with two different control strategies, the factors affecting the system stability differ from those observed when solely focusing on one control strategy, owing to the interaction among multiple trains, which remains unclear.

To fill this gap, this paper builds a unified impedance model of the train-network system

incorporating DQDC trains and TDCC trains. Then, the dominant eigenvalue frequency response criterion is proposed, capable of directly identifying the oscillation frequency and deeply analyzing the mechanism of LFO. On this basis, the interaction factors between different trains are revealed and the impact of the number and control parameters of trains on the global system stability are summarized by case studies and simulation verifications.

Unified impedance modeling

The structure of train-network system based on the combination of DQDC and TDCC topologies is shown in Fig. 1. The train's traction drive unit comprises of an on-board transformer, grid-side rectifier, traction inverter, and traction motor. Generally, the occurrence of LFOs is observed when multiple trains are energized in a rail depot, with only the auxiliary load in operation [1]. Hence, the DC-side of the traction drive unit can be equivalenced to a constant-value large resistance [3], whereas the impedance modeling of the train depends on the grid-side converter. The system parameters are shown in Table I.

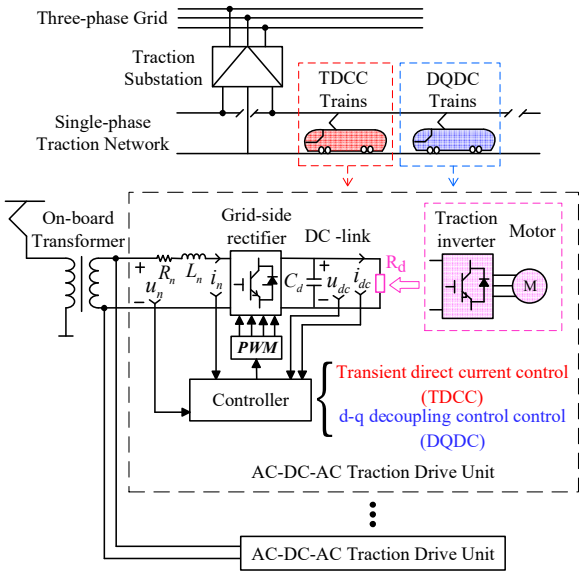

Fig. 1: Structure of train network system and train traction drive unit.

Fig. 2 and Fig. 3 illustrate the different control strategies, DQDC and TDCC, employed by the grid-side converter. Both strategies feature the key components such as the phase-locked loop (PLL), band-pass filter (BPF), second-order generalized integrator (SOGI), voltage controller (VC), and current controller (CC).

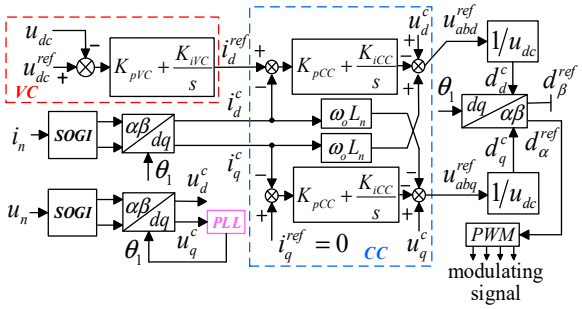

Fig. 2: Diagram of dq decoupling control (DQDC)
(VC : voltage controller, CC : current controller, PLL : phase-locked loop, SOGI : second-order generalized integrator).

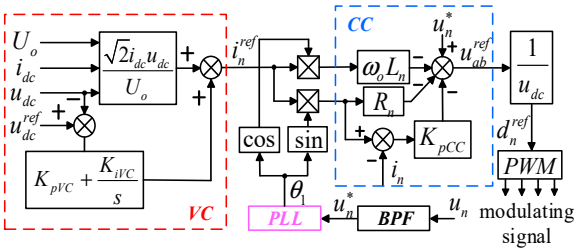

Fig. 3: Diagram of transient direct current control (TDCC) (BPF : band-pass filter).

Table I: Parameters of grid-side rectifier

Parameters	Variables /Unit	TDCC Train	DQDC Train
Amplitude of AC voltage	U_0 / V	2192	2503
DC link voltage	U_{dc} / V	3000	3600
Equivalent resistance on the AC side	R_n / Ω	0.15	0.165
Equivalent inductance on the AC side	L_n / mH	4	6
DC link load resistance	R_d / Ω	1000	1000
DC link support capacitance	C_d / mF	9	9
Time delay of PWM	T_d / ms	0.15	0.15
Switching Frequency	f_{sw} / Hz	350	250
Proportional gain of PLL	K_{pPLL}	0.7	0.7
Integral gain of PLL	K_{iPLL}	25	25

Proportional gain of VC	K_{pVC}	0.28	0.5
Integral gain of VC	K_{iVC}	20	0.8
Proportional gain of CC	K_{pCC}	0.2	0.9
Integral gain of CC	K_{iCC}	None	0.6

The modeling process of the second-order impedance model of the DQDC converter in the *dq* frame, $\boldsymbol{Z}_C^{DQDC}$, has been elaborated in [6]. As for the TDCC converter, to achieve the unification of frames, the modeling method in [9] can be used to realize impedance modeling in the *dq* frame. Therefore, $\boldsymbol{Z}_C^{DQDC}$ and $\boldsymbol{Z}_C^{TDCC}$ can finally be expressed as:

$$\boldsymbol{Z}_C^{DQDC} = \begin{bmatrix} z_{dd}^{DQDC} & z_{dq}^{DQDC} \\ z_{qd}^{DQDC} & z_{qq}^{DQDC} \end{bmatrix} \tag{1}$$

$$\boldsymbol{Z}_C^{TDCC} = \begin{bmatrix} z_{dd}^{TDCC} & z_{dq}^{TDCC} \\ z_{qd}^{TDCC} & z_{qq}^{TDCC} \end{bmatrix} \tag{2}$$

Considering the transformation ratio of the train's on-board transformer as *k*, and the number of grid-side converters in a train is *p*, where the subscripts "1" and "2" correspond to DQDC and TDCC train, the train impedance model converted to the primary side of the on-board transformer can be expressed as:

$$\boldsymbol{Z}_T = \begin{cases} \boldsymbol{Z}_T^{DQDC} = \dfrac{[(k_1)^2 \boldsymbol{Z}_C^{DQDC}]}{p_1}, & \text{with DQDC} \\ \boldsymbol{Z}_T^{TDCC} = \dfrac{[(k_2)^2 \boldsymbol{Z}_C^{TDCC}]}{p_2}, & \text{with TDCC} \end{cases} \tag{3}$$

When different types of trains are connected at the point of common coupling (PCC), the impedance of all trains can be connected in parallel equivalently like in [10] to form a unified train impedance model $\boldsymbol{Z}_{MT}$ as:

$$\boldsymbol{Z}_{MT} = (m_1(\boldsymbol{Z}_T^{DQDC})^{-1} + m_2(\boldsymbol{Z}_T^{TDCC})^{-1})^{-1} \tag{4}$$

where, m_1 and m_2 are the numbers of DQDC and TDCC trains.

Stability analysis criterion

Based on the impedance method, the train-network system in Fig. 1 can be regarded as a cascaded system as shown in Fig. 4. The equivalent impedance of the traction network can be expressed in the dq frame as [1]:

$$\boldsymbol{Z}_S = \begin{bmatrix} R_s + sL_s & -\omega L_s \\ \omega L_s & R_s + sL_s \end{bmatrix} \tag{5}$$

The open-loop impedance ratio matrix $\boldsymbol{L}_K$ of the cascaded system shown in Fig. 4 is:

$$\boldsymbol{L}_K = \boldsymbol{Z}_S(\boldsymbol{Z}_{MT})^{-1} \tag{6}$$

Both the traction network and train are stable respectively with reasonable parameter settings, meaning that the number of poles of $\boldsymbol{L}_K$ in the right half complex plane is zero [2]. According to the generalized Nyquist criterion (GNC), if the Nyquist curves corresponding to the two eigenvalues of $\boldsymbol{L}_K$, i.e., λ_{k1} and λ_{k2}, do not enclose the (-1, j0) point, the system is stable, otherwise, the system is unstable.

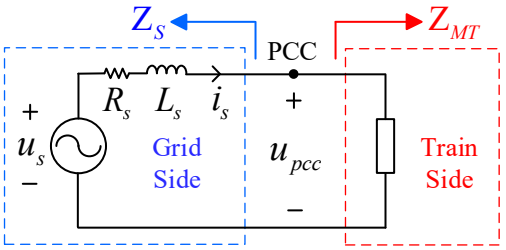

Fig. 4: Equivalent cascaded model of train-network system.

Proposed new stability criterion

A novel improved stability criterion can be proposed based on GNC. By adding the impedance ratio matrix $\boldsymbol{L}_K$ and the identity matrix $\boldsymbol{I}$, the matrix $\boldsymbol{L}_R$ can be obtained as :

$$\boldsymbol{L}_R = \boldsymbol{I} + \boldsymbol{L}_K \tag{7}$$

According to the eigenvalue formula of the second-order matrix, the two eigenvalues λ_{r1} and λ_{r2} of $\boldsymbol{L}_R$ are obtained as :

$$\lambda_{r1,r2} = 1 + \lambda_{k1,k2} \tag{8}$$

From (8), it can be seen that the real parts of λ_{r1} and λ_{r2} are one larger than that of λ_{k1} and λ_{k2}, while their imaginary parts are the same. Therefore, by considering the Nyquist curves based on $\lambda_{r1,r2}$, the assessment of the system stability can be performed by observing whether

the Nyquist curves surround the (0, j0) point, as shown in Fig. 5.

Actually, the system stability is determined by one of the eigenvalues, called the dominant eigenvalue λ_m, and the dominant eigenvalue λ_m in Fig. 5 is λ_{r1}. Moreover, the Nyquist curves of λ_m are the trajectory of the real and imaginary parts varying with frequency, which can be disassembled as $\mathrm{Re}[\lambda_m]=F_1(f)$ and $\mathrm{Im}[\lambda_m]=F_2(f)$, as shown in Fig. 6 across the vital low-frequency range of 0~10 Hz.

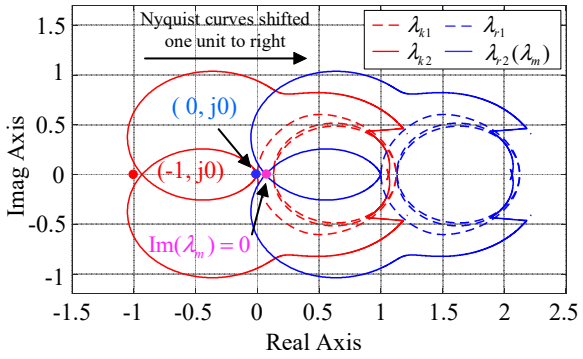

Fig. 5: Nyquist curves after transformation of impedance ratio matrix – Determine whether the Nyquist curves surround (0, j0) point.

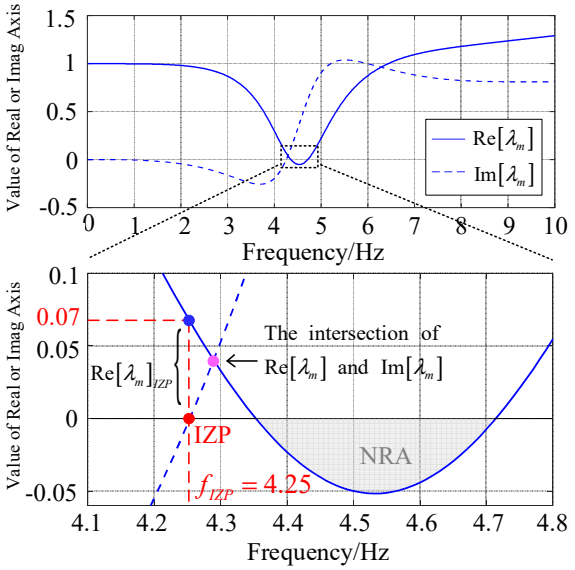

Fig. 6: Frequency response curves for the real and imaginary parts of the dominant eigenvalue – Definition of stability margin indicator $\mathrm{Re}[\lambda_m]_{IZP}$ (IZP : imaginary-part zero-crossing point, NRA : negative real-part area).

As shown in Fig. 5, $\mathrm{Im}[\lambda_m]$ is zero at the leftmost intersection of the Nyquist curve of λ_m with the real axis, which corresponds to the imaginary-part zero-crossing point (IZP) in Fig. 6. The frequency at IZP is denoted as f_{IZP}, and the real-part value of λ_m at f_{IZP} is $\mathrm{Re}[\lambda_m]_{IZP}$. In addition, there is a negative real-part area (NRA). Therefore, the proposed dominant eigenvalue frequency response criterion (DEFRC) can be expressed as if IZP is not included in the range of NRA, i.e., $\mathrm{Re}[\lambda_m]_{IZP}>0$, which corresponds to the Nyquist curve of λ_m without enclosing (0, j0) point, so the system is stable. On the contrary, if IZP is included in the range of NRA, i.e., $\mathrm{Re}[\lambda_m]_{IZP}<0$, the system is unstable.

It can be revealed by DEFRC that the oscillation frequency is the frequency corresponding to the intersection of $\mathrm{Re}[\lambda_m]$ and $\mathrm{Im}[\lambda_m]$. The relevant proving process will be given below. The stability of the system depends on the closed-loop poles, which are also the zeros of the determinant of $\boldsymbol{L}_R$. When the system is in a critically stable or unstable state, $\det[L_R]$ has a pair of conjugate zeros with very small negative or even positive real parts, which are called dominant zeros. Although $\det[L_R]=\lambda_{r1}\cdot\lambda_{r2}$, the dominant zeros are provided by λ_m. Therefore, it is assumed that λ_m has a pair of conjugate zeros in the low-frequency range: $\varepsilon_{1,2}=\sigma_{LFO}\pm j\omega_{LFO}$, and $|\sigma_{LFO}|\ll|\omega_{LFO}|$ [10]. When $j\omega$ is located in the tiny neighborhood of $\varepsilon_{1,2}$, λ_m can be expressed as:

$$\lambda_m(j\omega)=(j\omega-\varepsilon_1)(j\omega-\varepsilon_2)A(j\omega) \tag{9}$$

where, $A(j\omega)=a+jb$, and a & b are constants. Moreover, the real and imaginary parts of $\lambda_m(j\omega)$ can be obtained as:

$$\begin{cases}\mathrm{Re}[\lambda_m(j\omega)]=-a\omega^2+2b\sigma_{LFO}\omega+a(\sigma_{LFO}^2+\omega_{LFO}^2)\\ \mathrm{Im}[\lambda_m(j\omega)]=-b\omega^2-2a\sigma_{LFO}\omega+b(\sigma_{LFO}^2+\omega_{LFO}^2)\end{cases} \tag{10}$$

When $\mathrm{Re}[\lambda_m(j\omega)]=\mathrm{Im}[\lambda_m(j\omega)]$, the frequency ω_c at the intersection point of $\mathrm{Re}[\lambda_m]$ and $\mathrm{Im}[\lambda_m]$ is:

$$\omega_c=\frac{(a+b)\sigma_{LFO}}{(a-b)}\pm\frac{\sqrt{(a+b)^2\sigma_{LFO}^2+(a-b)^2(\sigma_{LFO}^2+\omega_{LFO}^2)}}{(a-b)} \tag{11}$$

Due to $|\sigma_{LFO}| \ll |\omega_{LFO}|$, it can be obtained that $\omega_c \approx \omega_{LFO}$, meaning the frequency corresponding to the intersection point of $\mathrm{Re}[\lambda_m]$ and $\mathrm{Im}[\lambda_m]$ is approximately the oscillation frequency.

Mechanism analysis of system stability

According to DEFRC, the value of $\mathrm{Re}[\lambda_m]_{IZP}$ serves as an indicator for the system stability margin, with its determination relying on the combined factors of $\mathrm{Re}[\lambda_m]$ and ω_{IZP}. Therefore, the effect of parameters on system stability can be dissected into their respective impacts on $\mathrm{Re}[\lambda_m]$ and ω_{IZP} ($\omega_{IZP} = 2\pi f_{IZP}$). This decomposition facilitates a thorough analysis of the underlying mechanism concerning parameter influence.

To be specific, if only TDCC trains are considered, there is $\boldsymbol{Z}_{MT} = \boldsymbol{Z}_T^{TDCC} / m_2$. The second-order impedance model of the TDCC converter in (2) can be simplified by the method proposed in [11]. After that, the approximate eigenvalues of $\boldsymbol{L}_R$ can be obtained as:

$$\begin{cases} \lambda_{r1} = 1 + \dfrac{m_2 p_2}{(k_2)^2} \dfrac{Z_{pp}^s}{Z_{pp}^c} \\ \lambda_{r2} = 1 + \dfrac{m_2 p_2}{(k_2)^2} \dfrac{Z_{nn}^s}{Z_{nn}^c} \end{cases} \tag{12}$$

In (12), Z_{pp}^s, Z_{nn}^s and Z_{pp}^c, Z_{nn}^c are the elements on the diagonal after $\boldsymbol{Z}_S$ and $\boldsymbol{Z}_C^{TDCC}$ are transformed to the modified sequence domain [12], which can be expressed as:

$$\begin{cases} Z_{pp}^s = R_s + j\omega L_s + j\omega_o L_s \\ Z_{nn}^s = R_s + j\omega L_s - j\omega_o L_s \end{cases} \tag{13}$$

$$\begin{cases} Z_{pp}^c = R_n + \dfrac{L_n}{T_d} + \dfrac{\omega_o L_n}{T_d \omega} + \dfrac{1}{2} R_{dd}^{tdcc} \\ \qquad + j[(\omega + \omega_o) L_n - \dfrac{R_n + K_{pCC}}{T_d \omega} + \dfrac{1}{2} R_{qd}^{tdcc}] \\ Z_{nn}^c = R_n + \dfrac{L_n}{T_d} - \dfrac{\omega_o L_n}{T_d \omega} + \dfrac{1}{2} R_{dd}^{tdcc} \\ \qquad + j[(\omega - \omega_o) L_n - \dfrac{R_n + K_{pCC}}{T_d \omega} - \dfrac{1}{2} R_{qd}^{tdcc}] \end{cases} \tag{14}$$

where, R_{dd}^{tdcc} and R_{qd}^{tdcc} are the negative resistance in the d-d and q-d components of the simplified impedance matrix of the TDCC converter, and they can be expressed as:

$$\begin{cases} R_{dd}^{tdcc} = -K_{pVC}(K_{pCC} + R_n) \dfrac{0.5 U_d}{T_d \omega^2 C_d U_{dc}} \\ R_{qd}^{tdcc} = -K_{pVC}(\omega_o L_n) \dfrac{0.5 U_d}{T_d \omega^2 C_d U_{dc}} \end{cases} \tag{15}$$

The combination of the simplified model with the proposed DEFRC enables the determination of the frequency value at which the imaginary part of the dominant eigenvalue becomes zero, denoted by ω_{IZP}. Then ω_{IZP} is inserted into the real part of the dominant eigenvalue, such that the calculation of the system stability margin indicator $\mathrm{Re}[\lambda_m^{tdcc}]_{IZP}$ can be expressed as :

$$\mathrm{Re}[\lambda_m^{tdcc}]_{IZP} = 1 + \frac{m_2 p_2}{(k_2)^2} \frac{(\omega_o - \omega_{IZP}) L_s}{(\omega_o - \omega_{IZP}) L_n + \dfrac{R_n + K_{pCC}}{T_d \omega_{IZP}} + \dfrac{R_{qd}^{tdcc}}{2}} \tag{16}$$

Within the low-frequency range, $\omega_o - \omega_{IZP} > 0$ holds, and if the consideration for negative resistance R_{qd}^{tdcc} is omitted, the stability margin indicator $\mathrm{Re}[\lambda_m^{tdcc}]_{IZP}$ will invariably remain above zero. Therefore, negative resistance makes the indicator of stability margin possibly negative. If some parameters are adjusted which amplifies the effect of negative resistance such that the stability margin indicator becomes negative, the LFO arises.

Table II: Impact of train numbers and control parameters on the system stability

Parameters	Sign	TDCC Train	DQDC Train
Number of trains	m	↓	↓
Proportional gain of PLL	K_{pPLL}	-	-
Integral gain of PLL	K_{iPLL}	-	-
Proportional gain of VC	K_{pVC}	↑	↓
Integral gain of VC	K_{iVC}	↓	↓
Proportional gain of CC	K_{pCC}	↑	↑
Integral gain of CC	K_{iCC}	×	↓

When it comes to the impact of parameters, it can be found from (16) that the number of TDCC

trains m_2 does not affect the value of ω_{IZP}, but the increase in m_2 can amplify the impact of the negative resistance, which will ultimately make $\mathrm{Re}[\lambda_m^{tdcc}]_{IZP}$ negative and lead to the instability of the system. In addition, the inclusion of control parameters K_{pVC} within R_{qd}^{tdcc} permits a similar assessment of its impact on system stability. For the sake of brevity, the results are presented herein without an elaborate analysis, showcasing that the increase in K_{pVC} leads to a reduction in ω_{IZP}, but eventually results in an increase in $\mathrm{Re}[\lambda_m^{tdcc}]_{IZP}$, enhancing the system stability.

In the case of solely considering DQDC trains, analogous derivation and analysis can be executed, which are not given in detail due to limited space. The impacts of the train number and control parameters on the system stability in non-mixed conditions are summarized in Table II, where '↑' and '↓' indicate that the system stability is improved or reduced with the increase of the corresponding parameter, '-' means no change in stability, and '×' means there is no such parameter.

In the consideration of mixed conditions involving trains with different controls, the derivation of further analytical expressions for the eigenvalues of $\boldsymbol{L}_R$ becomes arduous due to their excessive complexity, but some fundamental analysis can still be undertaken. Utilizing the matrix inversion formula, the determinant of $\boldsymbol{Z}_{MT}^{-1}$ can be obtained as:

$$D_T = \frac{m_1^2}{D_{DQDC}} + \frac{m_2^2}{D_{TDCC}} + \frac{m_1 m_2}{D_{TDCC} D_{DQDC}} D_E \tag{17}$$

where, D_{DQDC} and D_{TDCC} are the determinants of $\boldsymbol{Z}_T^{DQDC}$ and $\boldsymbol{Z}_T^{TDCC}$ respectively, and D_E is :

$$\begin{aligned} D_E = {} & z_{dd}^{TDCC} z_{qq}^{DQDC} + z_{dd}^{DQDC} z_{qq}^{TDCC} \\ & - z_{dq}^{TDCC} z_{qd}^{DQDC} - z_{dq}^{DQDC} z_{qd}^{TDCC} \end{aligned} \tag{18}$$

By combining (4) with (17), it can be obtained as:

$$\boldsymbol{Z}_{MT} = \left(\frac{\boldsymbol{Z}_T^{TDCC}}{m_1 + E_{DFT}}\right) + \left(\frac{\boldsymbol{Z}_T^{DQDC}}{m_2 + E_{TFD}}\right) \tag{19}$$

where, E_{DFT} and E_{DFT} are defined as the interaction factors between different trains, which can be expressed as:

$$\begin{cases} E_{DFT} = \dfrac{m_2}{D_{DQDC}} \left(\dfrac{m_2}{m_1} D_{TDCC} + D_E\right) \\ E_{TFD} = \dfrac{m_1}{D_{TDCC}} \left(\dfrac{m_1}{m_2} D_{DQDC} + D_E\right) \end{cases} \tag{20}$$

It can be seen from (19) that, under mixed conditions, the number and parameters of trains of a certain kind not only affect their own impedance but also the impedance of other trains through the interaction factor. As a result, the impact of the number and parameters on the system stability becomes multifaceted, which will be demonstrated by case studies in the next section.

Case studies and validation

As shown in Fig. 7, when TDCC trains are solely considered, as the number of trains m_2 increases from 4 to 8, the ω_{IZP} remains unchanged at 4.25 Hz, while $\mathrm{Re}[\lambda_m^{tdcc}]_{IZP}$ gradually decreases. When m_2 increases to 8, NRA appears in the low-frequency range and $\mathrm{Re}[\lambda_m^{tdcc}]_{IZP}$ decreases to -0.063, which means that the system becomes unstable. At this point, the predicted oscillation frequency is about 4.22 Hz.

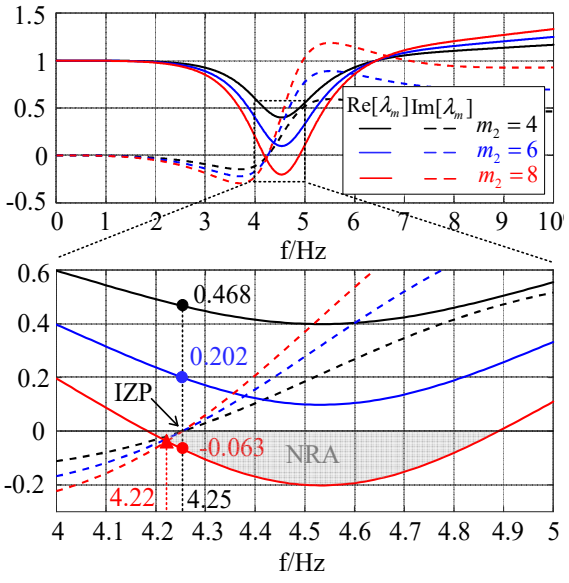

Fig. 7: Stability analyses with the DEFRC – System stability decreases when the number of TDCC trains increases.

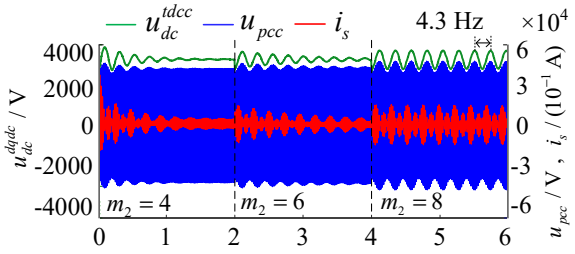

Fig. 8: Waveforms showing destabilization when the number of TDCC trains increases from 4 to 8.

Fig. 8 presents the simulation waveform, encompassing the voltage and current of the traction network, along with the DC side voltage of the converter. When m_2 attains 8, LFO occurs at a frequency of 4.3 Hz. The results obtained from the case study and simulation demonstrate a strong consistency with the theoretical analysis, presenting only a slight error in the oscillation frequency due to the approximation in (9).

In Fig. 9, the values of $\mathrm{Re}[\lambda_m]_{IZP}$ are presented for various combinations of train numbers in mixed conditions. The numbers of TDCC and DQDC trains vary from 1 to 8, respectively. It remains valid in mixed conditions, that the decrease in the system stability as the number of trains increases. Moreover, when the number of trains reaches 8 in non-mixed conditions, the system is unstable. However, in mixed conditions, even in some cases with a total of 8, 9, or 10 trains, the system remains stable. This improvement in the critically stable number of trains in mixed conditions highlights the advantage of avoiding excessive single type trains energized in the same depot, and enhancing the system stability.

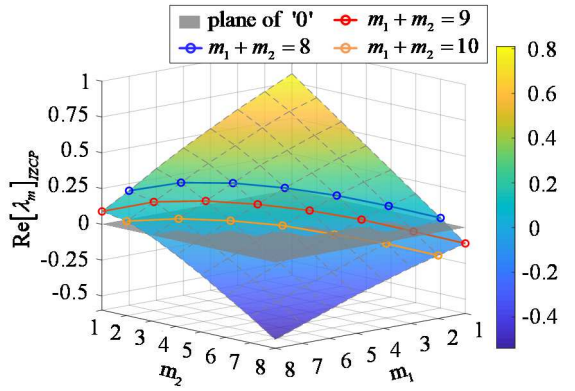

Fig. 9: Indicator of stability margin under various train numbers. – The critically stable number of trains is improved when considering different trains.

As for the influence of control parameters, as shown in Fig. 10, when $m_1 = 6$ and $m_2 = 5$, as the VC proportional gain of the DQDC train K_{pVC}^{dqdc} increases from 0.5 to 2.2, the range of NRA is greatly reduced, while IZP changes in a smaller range without regularity, and $\mathrm{Re}[\lambda_m]_{IZP}$ increases from -0.041 to 0.132, indicating the system stability is improved. However, Fig. 11 shows when $m_1 = 7$ and $m_2 = 1$, as K_{pVC}^{dqdc} increases from 0.5 to 0.9, the range of NRA decreases slightly, while IZP moves greatly closer to the NRA, resulting in a decrease of $\mathrm{Re}[\lambda_m]_{IZP}$ from 0.204 to -0.103, which means a decrease in system stability.

The results presented above reveal that when considering different combinations of train numbers, the variation of $\mathrm{Re}[\lambda_m]_{IZP}$ differs as K_{pVC}^{dqdc} increases, leading to either a positive or negative impact on the system stability, which is an uncertainty. This conclusion applies to other parameters as well. Therefore, under mixed conditions, a detailed analysis must be conducted based on the varying combinations of train numbers to obtain the influence rules of the parameters, allowing for informed adjustments to improve the system stability.

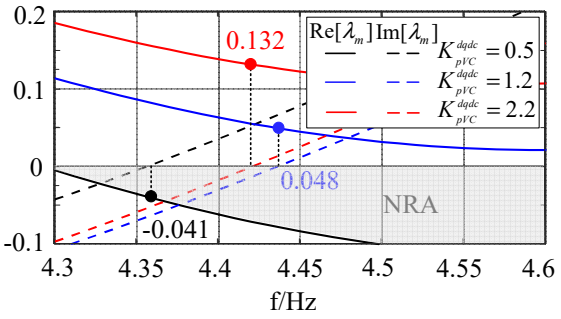

Fig. 10: System stability enhances as K_{pVC}^{dqdc} increases, when $m_1 = 6$ and $m_2 = 5$.

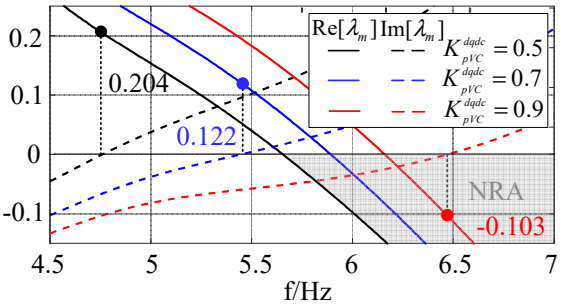

Fig. 11: System stability weakens as K_{pVC}^{dqdc} increases, when $m_1 = 7$ and $m_2 = 1$.

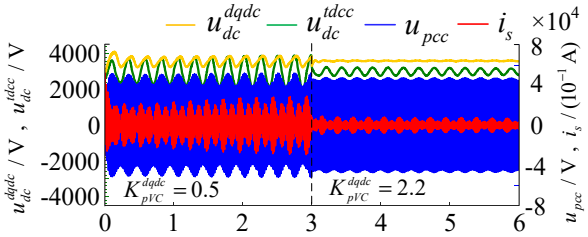

Fig. 12: Simulation waveforms stabilize as K_{pVC}^{dqdc} increases, when $m_1 = 6$ and $m_2 = 5$.

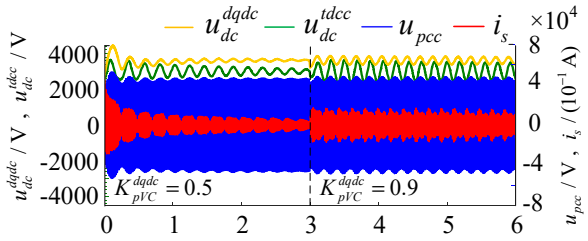

Fig. 13: Simulation waveforms destabilize as K_{pVC}^{dqdc} increases, when $m_1 = 7$ and $m_2 = 1$.

The simulation results as shown in Fig. 12 and Fig. 13 verify that the impact of K_{pVC}^{dqdc} on the system stability exhibits an opposite trend in two situations. Additionally, it is observed that under the condition of $m_1 = 7$ and $m_2 = 1$ with initial parameters, despite a total of 8 trains, the system remains stable. Hence, the simulation results are in agreement with the findings of the case analysis.

Conclusion

This paper establishes a unified impedance model of the train-network system incorporating different control strategies in the dq frame. Then, the dominant eigenvalue frequency response-based criterion is proposed, facilitating the prediction of oscillation frequency and the provision of a stability margin indicator, which elucidates that the negative resistance is the root cause of instability. Furthermore, the interaction between different trains in mixed conditions highlights the complex characteristics of parameter impact on the system stability. Case studies illustrate that under mixed conditions, the critically stable number of trains is improved and the impact of control parameters on system stability varies depending on the specific combination of train numbers.

References

[1] H. Hu, Y. Zhou, X. Li and K. Lei, "Low-Frequency Oscillation in Electric Railway Depot: A Comprehensive Review," *IEEE Trans. Power Electron.*, vol. 36, no. 1, pp. 295-314, 2021.

[2] H. Wang, M. Wu and J. Sun, "Analysis of Low-Frequency Oscillation in Electric Railways Based on Small-Signal Modeling of Vehicle-Grid System in dq Frame," *IEEE Trans. Power Electron.*, vol. 30, no. 9, pp. 5318-5330, 2015.

[3] H. Hu, H. Tao, F. Blaabjerg, X. Wang, Z. He and S. Gao, "Train–Network Interactions and Stability Evaluation in High-Speed Railways–Part I: Phenomena and Modeling," *IEEE Trans. Power Electron.*, vol. 33, no. 6, pp. 4627-4642, 2018.

[4] H. Zhang, Z. Liu, S. Wu and Z. Li, "Input Impedance Modeling and Verification of Single-Phase Voltage Source Converters Based on Harmonic Linearization," *IEEE Trans. Power Electron.*, vol. 34, no. 9, pp. 8544-8554, 2019.

[5] X. Wang and F. Blaabjerg, "Harmonic Stability in Power Electronic-Based Power Systems: Concept, Modeling, and Analysis," *IEEE Trans. Smart Grid.*, vol. 10, no. 3, pp. 2858-2870, 2019.

[6] Y. Liao, Z. Liu, H. Zhang and B. Wen, "Low-Frequency Stability Analysis of Single-Phase System With dq-Frame Impedance Approach—Part I: Impedance Modeling and Verification," *IEEE Trans. Ind. Applicat.*, vol. 54, no. 5, pp. 4999-5011, 2018.

[7] X. Jiang, H. Hu, X. Yang, Z. He, Q. Qian and P. Tricoli, "Analysis and Adaptive Mitigation Scheme of Low-Frequency Oscillations in AC Railway Traction Power Systems," *IEEE Trans. Transp. Electrific.*, vol. 5, no. 3, pp. 715-726, 2019.

[8] Z. Liu, G. Zhang and Y. Liao, "Stability Research of High-Speed Railway EMUs and Traction Network Cascade System Considering Impedance Matching," *IEEE Trans. Ind. Applicat.*, vol. 52, no. 5, pp. 4315-4326, 2016.

[9] R. Kong, X. Lv and X. Wang, "Low-Frequency Oscillation Analysis of Train-Network System with Different Types of Trains Connected," *IEEE Conf. Ind. Electron. Appl. ICIEA*, pp. 1530–1535, 2021.

[10] H. Liu, X. Xie and W. Liu, "An Oscillatory Stability Criterion Based on the Unified dq-frame Impedance Network Model for Power Systems with High-Penetration Renewables," *IEEE*

Trans. Power Electron., vol. 33, no. 3, pp. 3472-3485, 2018.

[11] Y. Zhou, H. Hu, X. Yang, J. Yang, Z. He and S. Gao, "Low Frequency Oscillation Traceability and Suppression in Railway Electrification Systems," *IEEE Trans. Ind. Applicat.*, vol. 55, no. 6, pp. 7699-7711, 2019.

[12] A. Rygg, M. Molinas, C. Zhang, and X. Cai, "A modified sequence domain impedance definition and its equivalence to the dq-domain impedance definition for the stability analysis of ac power electronic systems," *IEEE J. Emerg. Sel. Top. Power Electron.*, vol. 4, no. 4, pp. 1383-1396, 2016.